Molecular Dynamics Simulations of the Interactions between Platinum Clusters and Carbon Platelets

**Carlos F. Sanz-Navarro,*,† Per-Olof Åstrand,† De Chen,‡ Magnus Rønning,‡
Adri C. T. van Duin,§ Timo Jacob,# and William A. Goddard, III§**

*Department of Chemistry, Norwegian University of Science and Technology (NTNU), 7491 Trondheim,
Norway, Department of Chemical Engineering, Norwegian University of Science and Technology (NTNU),
7491 Trondheim, Norway, Materials and Process Simulation Center, Division of Chemistry and Chemical
Engineering, California Institute of Technology, Pasadena, California 91125, and Fritz-Haber-Institut der
Max-Planck-Gesellschaft, Faradayweg 4-6, D-14195 Berlin, Germany*

Molecular dynamics simulations have been performed with two reactive force fields to investigate the structure of a Pt_{100} cluster adsorbed on the three distinct sides of a carbon platelet. A revised Reax force field for the carbon−platinum system is presented. In the simulations, carbon platelet edges both with and without hydrogen termination have been studied. It is found that the initial mismatch between the atomic structure of the platelet egde and the adsorbed face of the Pt_{100} cluster leads to a desorption of a few platinum atoms from the cluster and the subsequent restructuring of the cluster. Consequently, the average Pt−Pt bond length is enlarged in agreement with experimental results. This change in the bond length is supposed to play an important role in the enhancement of the catalytic activity, which is demonstrated by studying the changes in the bond order of the platinum atoms. We found an overall shift to lower values as well as a loss of the well-defined peak structure in the bond-order distribution.

1. Introduction

Hydrogen-fueled proton exchange membrane (PEM) fuel cells can efficiently convert chemical energy to electricity with water as the only byproduct. The reverse process, namely electrolysis of water, has long been used for hydrogen production.[1] Platinum occupies a privileged position in the list of catalysts for both processes.[2] It is, however, an expensive metal, which increases the cost of production of electrocatalytical cells. As an alternative, Pt clusters of a radius of a few nanometers placed on a supporting material have attracted interest as catalysts because the surface−volume ratio is maximized as the size is reduced.[3] In addition, different cluster supports have been considered. Among these, carbon is the best choice for the supports of electrocatalysts due to high surface area, inertness in basic and acidic solution and high conductivity. In particular, carbon nanotubes (CNT) and carbon nanofibers (CNF) has attracted great attention due to their unique structural, mechanical and electronic properties.[4] Superior performances of CNT and CNF supported Pt and alloy catalysts have been observed experimentally.[5−7] Recently an enhanced catalytic activity of Ni clusters adsorbed on carbon nanostructured materials has been measured,[8] which has been ascribed to an expansion of nanoparticles induced by CNF. The actual structure of a metal cluster after being adsorbed on a carbon nanofiber and how this affects the catalytic properties of the cluster is, however, challenging to study experimentally with a resolution on the atomistic level.[9]

This explains the role played by atomistic simulations in this field which can be utilized to investigate the structural transformations of a metal cluster adsorbed on a surface support.

In heterogeneous catalysis and surface science, density functional theory (DFT) calculations have provided detailed insight of the atomic and electronic structure of the entities involved in the processes.[10−12] For example, the interaction between a Pt atom and 1−2 graphite planes[13] and the stabilization of Pt_n ($n =1,6$) by boron-doped carbon structures[14] have recently been studied. In some cases, DFT has been combined with molecular dynamics (MD) simulations, but these studies are so far restricted to relatively small systems and short times.[15,16] If force fields are employed,[17,18] the calculations of energies and forces are very fast compared to quantum-chemical calculations. A force field, however, relies on a choice of the functional form of the potential function and on a parametrization of a data set to obtain the force fields parameters. Nonetheless, if a suitable functional form is chosen and data obtained from quantum-chemical calculations are used in the parametrization, it is expected that the force field mimics the potential surface of the corresponding quantum-chemical method. Most force fields are nonreactive and models of covalent bonding are included explicitly through bond stretch, angle bending and torsional terms. In a reactive force field, however, all atom−atom interactions in the system have to be treated on an equal footing because the molecular composition cannot be known *a priori*. One way to derive reactive force fields is to use a bond-order approach,[19] where all the short-range energy terms depend explicitly on the atomic bond orders. Two of the most widely employed bond-order force fields are the Brenner force field (BrennerFF) and the Reax force field (ReaxFF). The BrennerFF was originally proposed to describe the interatomic interactions in hydrocarbons.[20] Then the same formulation has

  * Corresponding author. E-mail: carlos.sanz@ntnu.no.
  † Department of Chemistry, Norwegian University of Science and Technology.
  ‡ Department of Chemical Engineering, Norwegian University of Science and Technology.
  § California Institute of Technology.
  # Fritz-Haber-Institut der Max-Planck-Gesellschaft.

MD of Pt Cluster−C Platelet Interactions

J. Phys. Chem. A, Vol. 112, No. 7, 2008 **1393**

been extended to model the interatomic interactions in systems made up of C/Si/H,[21] C/H/O,[22] Zi/O,[23] W/C/H,[24] Si/C,[25] Ga/Ni,[26] and Pt/C.[27] On the other hand, the ReaxFF is based on a bond-order model in conjunction with a charge-equilibration scheme,[28] and it was also first developed for hydrocarbons.[29] Subsequently, the ReaxFF has been extended to many other elements and compounds such as Si/SiO$_2$,[30] Al/AlO,[31] Ni/Cu/Co/C,[32] Mg/MgH,[33] Li/LiC,[34] and BiMoO$_x$.[35]

The purpose of this work is to investigate the structural changes as well as the strain induced in the bond length of a Pt$_{100}$ cluster upon adsorption on a carbon platelet. First the methodology is described, both for the parametrization of the ReaxFF and for the simulations. Then the revised C/Pt/H ReaxFF is presented and a comparison of a BrennerFF and the new ReaxFF is given for a simulation of a Pt$_{100}$ interacting with the armchair edge of the graphene sheets. Finally, the ReaxFF has been adopted to study the interaction of the Pt cluster at different types of graphite edges and for different degrees of hydrogen termination.

2. Methodology

2.1. Reactive Force Fields. We have employed two different force fields to model the interatomic interactions. First, we have adopted a BrennerFF parametrized by Albe et al.[27] to describe the short-range interatomic interactions in C/Pt systems. The analytical expression of the BrennerFF energy consists of a cutoff function, f_{ij}, a repulsive term, V_R, an attractive term, V_A, and a bond-order term, B_{ij}, so that the energy of the whole system is given as

$$E = \sum_{i<j} f_{ij}(r_{ij})[V_R^{ij}(r_{ij}) - B_{ij}V_A^{ij}(r_{ij})] \qquad (1)$$

Details of the analytical form for each of the terms considered in eq 1 and the C/Pt parameters obtained by fitting against DFT data of dimers and periodic systems are found in ref 27. In conjunction with the BrennerFF, a Lennard-Jones potential has been considered to mimic the weak van der Waals interactions between the carbon atoms of adjacent layers.[36]

Second, we have considered a ReaxFF for C/Pt/H systems. The ReaxFF energy is written as a sum of distinct contributions,

$$E_{system} = E_{bond} + E_{val} + E_{tors} + E_{Coulomb} + E_{vdWaals} + E_{coa} + \\ E_{conj} + E_{lp} + E_{pen} + E_{under} + E_{over} \quad (2)$$

where the bond (E_{bond}), valence angle (E_{val}), dihedral (E_{tors}), Coulomb ($E_{Coulomb}$) and van der Walls ($E_{vdWaals}$) interactions are considered as well as energy terms for three-body conjugation (E_{coa}), four-body conjugation (E_{conj}), lone pairs (E_{lp}) and penalty terms for stabilization of systems with two double bonds sharing an atom in a valency angle (E_{pen}), undercoordinated (E_{under}) and overcoordinated (E_{over}) atoms. The bonded interactions depend explicitly on a bond-order term (BO$_{ij}$) that includes contributions from single, double and triple bonds. The specific analytical expression of each of the energy contributions in eq 2 along with a detailed explanation of the physical meaning can be found in ref 29 and the Supporting Information of ref 32. Furthermore, atomic charges are recalculated at each step of the simulation using a charge-equilibration scheme,[28] so that the eletrostatic interactions are environmentally dependent as required during formation and breaking of bonds. To optimize the force field parameters, DFT calculations have been performed using periodic systems and finite clusters. For the Pt−Pt interactions bulk and slab calculations were performed using SeqQuest,[37,38] a periodic DFT program with Gaussian basis sets,

with the PBE[39] generalized gradient approximation (GGA) exchange−correlation (xc) functional and norm-conserving pseudopotentials to replace the core electrons.[40] On the basis of this approach, we performed calculations on the equation-of-states for various bulk structures (fcc, bcc, sc, and a-15) as well as the stability of various surface orientations. Besides the structural and energetical information from these studies, equivalent values for finite Pt clusters (up to 35 atoms) were used in the force field optimization procedure.[41,42] The quantum-mechanical results on the finite systems, including pure Pt clusters and various CH$_x$ and C$_2$H$_y$ hydrocarbons adsorbed on Pt, were obtained by spin-unrestricted DFT calculations with the B3LYP hybrid xc-functional[43,44] using the Jaguar program suite,[45] in which the Pt-core electrons were replaced by an effective core-potential (ECP)[46] and the valence electrons were treated explicitly using the LACVP** basis set. The 6-31G** basis set was considered for the electrons in the C and H atoms.

2.2. Simulation Details. The BrennerFF simulations have been performed using the LBOMD code,[47] with the additional implementation of the force field. A time step of 1 fs was used in these simulations, which was checked to be enough to conserve the energy of the system in simulations of the microcanonical ensemble. On the other hand, all the ReaxFF simulations have been carried out with the ReaxFF code, with the minor addition of the Nosé−Hoover chain thermostat.[48] A few trial ReaxFF simulations in the microcanonical ensemble showed that a shorter time step of 0.25 fs is necessary to conserve the energy of the system, which is caused by the charge-equilibration scheme. Therefore, we use such a small time step during the ReaxFF simulations at constant temperature.

A cluster of 100 Pt atoms has been selected to mimic structural changes in a real cluster because this size is approximately halfway between two highly symmetric clusters: Pt$_{55}$ and Pt$_{147}$.[49] The diameter of a Pt$_{100}$ cluster is ∼2 nm, which is within the cluster size investigated experimentally for fuel cell catalysis applications (i.e., 1−5 nm).[5,7,50] The initial structure of the Pt$_{100}$ cluster was found by an energy minimization based on a genetic algorithm (GA).[51]

The carbon platelets were built by creating a small graphite slab with a distance of 1.42 Å between carbon atoms within each graphitic layer, which is the distance between first neighbor atoms in graphite.[52] The interlayer distance was quite close to that of graphite (i.e., 3.41 Å[52]), although the actual value was found by miminization of the potential energy with respect to the graphite interlayer distance to improve the stability of the system during the simulations. The values found were 3.398 Å for the long-range interactions added to the BrennerFF and 3.260 Å for the ReaxFF. Four different graphite lattices were built, bearing in mind the specific cluster−sheet binding edge, the interaction range and the computational cost of the force field employed. However, in all the cases the graphite planes were perpendicular to the *y*-axis and periodic boundary conditions were applied along the *x*- and *y*-directions. Details about the four graphite lattice are (1) A 10-layer graphite lattice with dimensions of 29.826 Å × 30.582 Å × 28.290 Å was considered for the BrennerFF simulation of the binding of a Pt$_{100}$ cluster on the armchair edge. Each graphite layer contained 336 carbon atoms. The armchair edge was perpendicular to the *z*-axis. This graphite lattice was placed inside a simulation box with dimensions of 29.286 Å × 33.980 Å × 50.0 Å to have periodic boundary conditions only in the *x*- and *y*-directions. (2) A 10-layer lattice with dimensions of 29.826 Å × 29.340 Å × 28.290 Å was employed in the ReaxFF simulation of the binding of a Pt$_{100}$ cluster to the armchair edge. Each graphite layer contained

1394 *J. Phys. Chem. A, Vol. 112, No. 7, 2008*

Sanz-Navarro et al.

336 carbon atoms. The sheets were oriented in the same way as for the BrennerFF simulation. This lattice was located within a simulation box with dimensions 29.826 Å × 32.60 Å × 50.0 Å. (3) A 10-layer graphite lattice with dimensions of 29.52 Å × 29.340 Å × 29.83 Å was employed for the simulations of a Pt$_{100}$ cluster adsorbed onto the zigzag edge of a carbon platelet, where the zigzag edge was perpendicular to the *z*-direction. Each graphite layer contained 360 atoms. This graphite lattice was introduced in a simulation box with dimensions 29.52 Å × 32.60 Å × 50.0 Å. (4) A 4-layer thin graphite layer with dimensions of 45.510 Å × 9.78 Å × 44.029 Å was chosen for the interaction between the Pt$_{100}$ cluster and the basal plane of a graphite surface. Each graphite layer contained 836 atoms. This graphite lattice was located inside a simulation box with dimensions of 45.510 Å × 50.0 Å × 44.029 Å. Periodic boundary conditions were applied along the directions parallel to the graphite planes.

The Pt$_{100}$ cluster was initially placed at a typical C−Pt distance of around 2 Å away from the platelet and then the overall energy of the system was minimized without constraints. Afterward, the system was subjected to an initial period of thermal equilibration at 600 K. First, a Berendsen thermostat[53] was used to achieve a fast convergence of the system temperature to the target value. A Nosé−Hoover chain thermostat[48] was used subsequently to obtain a proper NVT ensemble over a period of a million MD steps.

We have investigated the changes in the local structure surrounding a cluster atom by means of a common-neighbor-analysis (CNA) approach[54] as well as the bond-length and bond-order distribution. We have also calculated the strain in the bond length expressed as

$$\text{strain} = \frac{d_{\text{strained}} - d_{\text{unstrained}}}{d_{\text{unstrained}}} \quad (3)$$

where d_{strained} and $d_{\text{unstrained}}$ denote the strained and unstrained bond length, respectively. Both Pt−Pt and C−Pt bonds have been taken into account in the analysis. To be consistent in our criterion to define first neighbors, we have always considered the cutoff ranges defined in the BrennerFF,[27] i.e. a covalent bond of 3.3 Å for Pt−Pt and 2.8 Å for C−Pt. The specific expression employed for the computation of the bond order depends on the force field employed during the simulations. The ReaxFF considers Pauling's bond-distance dependence for the calculation of the bond order, whereas the bond-order term in the BrennerFF has a more complex expression, which also includes three-body terms. The bond-order distributions have only been calculated for atoms of the cluster surface that are exposed to the environment because these changes in this distribution can be related to changes in the catalytic performance of the cluster.[55] From now on, we will denote this subset of Pt atoms "as exposed cluster surface". In particular, a reduction in the bond order of the atoms will result in an enhancement of the capability of the cluster to bind surrounding atoms, leading to an increased catalytic activity of the cluster. To identify the solvent-accessible cluster surface, we have employed an algorithm similar to that implemented in the MSMS program.[56] Some details of our algorithm are schematically explained in Figure 1.

All the analyzed properties of the systems have been calculated by averaging data derived from the atom positions that were recorded at a frequency of 25 fs. The statistical error has been calculated by the root-mean-square deviation in the sample. We found the same autocorrelation time for both the bond-length and bond-order ditribution for each force field,
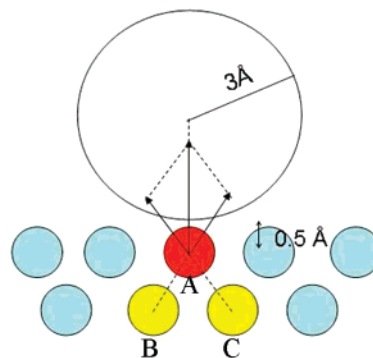

Figure 1. Exposed Pt-surface atoms identified by an algorithm similar to that employed in the MSMS program.[56] The sum of the vectors pointing from two nearest-neighbors atoms (B and C) to a given atom (A) defined a direction along which a sphere of a radius of 3 Å was located at a distance of 3.5 Å away from atom A. If no atom was found inside such a sphere, then atom A was considered to belong to the accessible-solvent cluster surface. The same process was repeated for each platinum atom and pair of first nearest neighbor atoms.

although slightly different between force fields: ∼6 fs for the BrennerFF and ∼10 fs for the ReaxFF, which are both very small values. In contrast, the CNA signature is rather stable to small changes in the local structure, so the number of hits for each value of the CNA distribution changes over time scales of the order of 100 fs and this gives much larger autocorrelation times. Therefore, we group the recorded data in 0.5 ps bins to ensure sufficiently autocorrelated samples for the calculation of the statistical error as well as to obtain a sufficiently large number of samples to make a proper average.

3. Results and Discussion

3.1. Parametrization of the ReaxFF. The ReaxFF Pt/C/H parameters were optimized against a training set of binding structures and adsorption energies obtained from DFT calculations on the chemisorption of all CH$_x$ and C$_2$H$_y$ hydrocarbons on Pt(111).[57] In these DFT studies, we found that all the hydrocarbons bind covalently such that a configuration is achieved in which each C is almost tetrahedrally structured with the missing H atoms replaced by covalent bonds to surface Pt atoms (see Figure 2). Thus, CH and vinyl prefer fcc hollow sites, CH$_2$ prefers a bridge site, and CH$_3$ prefers on-top binding. The only exceptions are ethynyl (CCH) and HCCH, which retain their C=C π-bonds while being located at fcc hollow sites. With respect to the binding strength we find that the most strongly bound CH$_x$ species is methylidyne (CH, BE = 146.61 kcal/mol), and ethylidyne (CCH$_3$, BE = 134.83 kcal/mol) among the C$_2$H$_y$ molecules. In addition it turned out that the net bond energy is nearly proportional to the number of C−Pt bonds (48.80 kcal/mol per bond) with the average bond energy decreasing slightly with the number of C ligands. The ReaxFF C/H parameters were trained against the entire hydrocarbon training set,[29] thus ensuring full transferability with earlier reported Reax parameters.

Besides these most stable surface sites for the adsorbates, we also considered less favorable positions, which might be relevant under conditions of higher surface coverages. In addition, this allowed us to include into the force field the ability to distinguish different hybridizations within the hydrocarbons and when binding to Pt(111).

The full set of ReaxFF parameters are available in the Supporting Information.

3.2. Comparison between the BrennerFF and the ReaxFF Simulations. Two simulations without hydrogen termination,
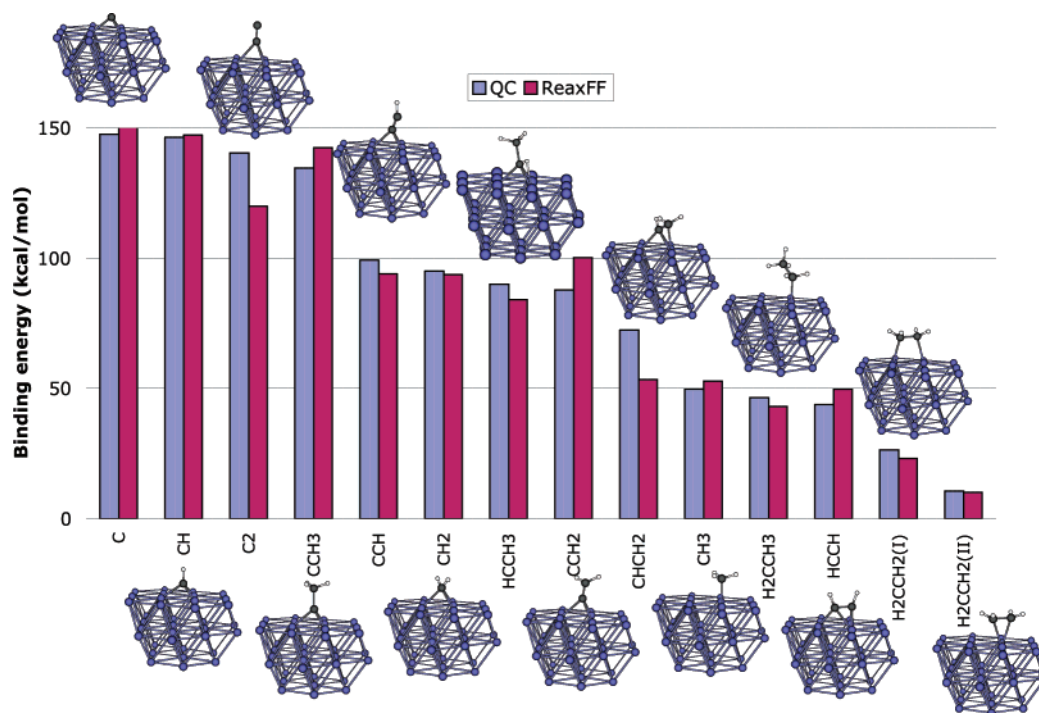
MD of Pt Cluster−C Platelet Interactions

J. Phys. Chem. A, Vol. 112, No. 7, 2008 **1395**

Figure 2. DFT and ReaxFF hydrocarbon binding energies to a Pt_{35} cluster.
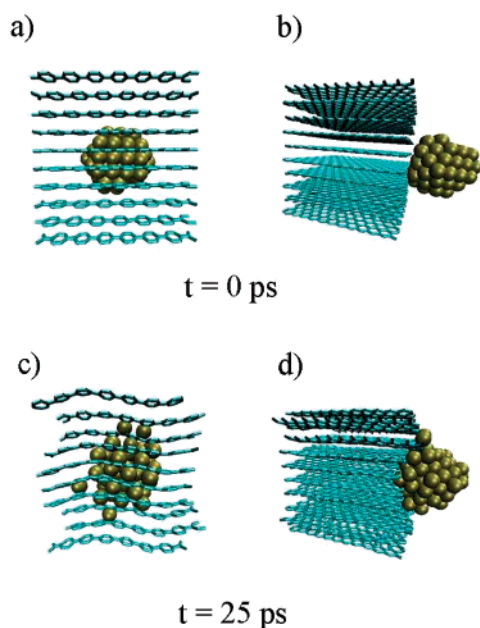

Figure 3. Reax simulation of a Pt_{100} cluster interacting with the armchair edge of the carbon platelet without hydrogen termination. (a) and (b) show the initial configuration from two directions. (c) and (d) show a snapshot after 25 ps of equilibration.

one using the BrennerFF and one with the ReaxFF, have been performed to investigate the structural changes in a Pt_{100} cluster adsorbed on the armchair-shaped edge of a graphite platelet. The Pt_{100} cluster minimized by the GA has a layered structure with a spacing of 2.79 Å in such a way that at least three layers of the cluster structure can be initially made to nearly coincide with the graphite interlayer spacing as shown in Figure 3. During the equilibration stage, the structure of the Pt_{100} cluster remained quasi-intact for the BrennerFF, and the cluster flattened and to some extent spread over the graphite edge for the ReaxFF (Figure 3).

The mean CNA distribution is displayed in Figure 4 for an isolated cluster and for the cluster attached to the graphite

platelet using the two force fields. The CNA distribution hardly changes for the BrennerFF. For the ReaxFF, however, the initial partial fcc-like structure is nearly lost as a result of the adsorption on the carbon substrate. In particular, nearly 90% of the atoms have an unclassified local structure. Differences between the simulations using each force field are also notable by comparing the respective bond-length distributions. The Pt−Pt bond-length distribution over the surface atoms of the Pt_{100} cluster is presented in Figure 5. For the BrennerFF, the mean bond length is 2.743 Å for the isolated cluster and 2.758 Å for the adsorbed cluster, which gives a Pt−Pt strain of 5.8×10^{-3} as calculated by eq 3. For the ReaxFF, the mean bond length is 2.847 Å for the isolated cluster and 2.888 Å for the adsorbed cluster, which leads to a Pt−Pt strain of 0.014. To our knowledge, there are not yet published experimental precise data on strain for platelet-adsorbed Pt clusters of size of 2 nm or larger. In contrast, values of induced strain in Ni clusters adsorbed on carbon supports derived from XRD spectra have been reported.[8] In such a study, the induced strain in the bond length for Ni clusters adsorbed on a carbon platelet is ∼0.025, which is of the same order of magnitude as the value reported above for the ReaxFF induced strain in the Pt−Pt bond.

Because the bond-order of an atom is a function of both the bond length and the number of neighboring atoms, major changes in the bond-order distribution for the surface Pt atoms are found for the ReaxFF (Figure 6). Initially, the Pt bond-order distribution presents well-defined and pronounced peaks, but after adsorption, the distribution is unstructured. Moreover, an increase in the probability distribution for lower bond orders and a correspondent reduction in the probability of higher values is found. Therefore, in comparison to the BrennerFF, the ReaxFF predicts a more enhanced catalytic activity of the Pt_{100} cluster as a result of the binding to the graphite sheets.

A remarkable difference between both force fields is the preferential sites where the Pt atoms get adsorbed. The Pt atoms have preference for 2-fold coordinated binding sites located on the plane of a graphite sheet in the BrennerFF simulation, whereas a 4-fold coordinated binding site at the interlayer space
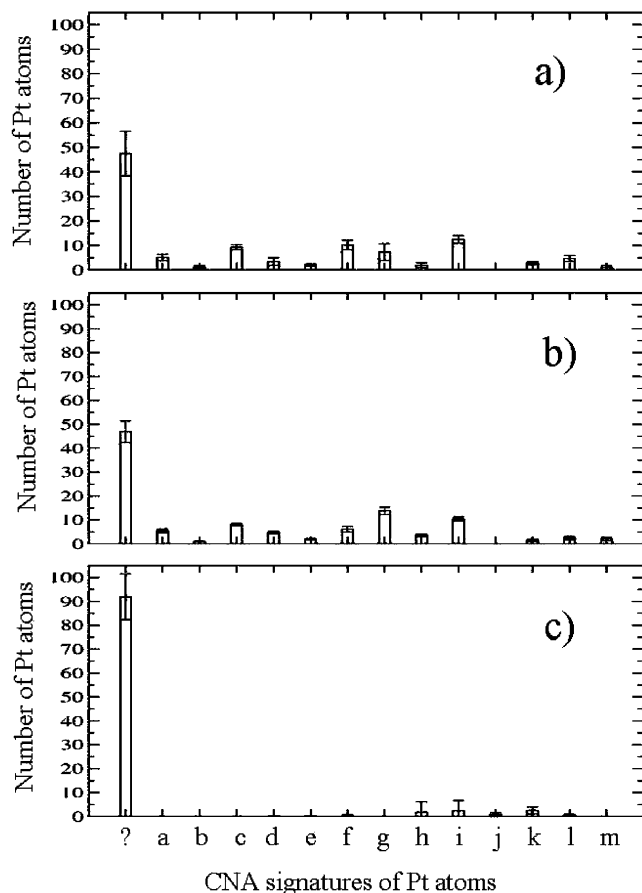
Figure 4. Distributions of the mean local structure of the Pt cluster atoms. (a) Distribution for an isolated Pt cluster modeled by the ReaxFF. (b) Distribution for the cluster−platelet system modeled by the Brenner force field. (c) Distribution for the cluster−platelet system by the ReaxFF simulation. A full explanation of the notation employed to represent local structure by CNA signatures can be found in ref 82. Briefly, "?" denotes a local structure different than any of the following ones, "a" fcc bulk, "b" fcc (100) surface, "c" fcc (111) surface, "d" fcc (111)−(100) edge, "e" fcc(111)−(111) edge, "f" truncated octahedron, "g" icosahedral internal twinning plane, "h" icosahedral spine, "i" icosahedral surface edge, "j" icosahedral central atom, "k" icosahedral surface vertex or decahedral notch vertex, "l" truncated icosahedral vertex or decahedral notch vertex, and "m" decahedral notch edge.

is the preferential binding site for the adsorbed Pt atoms in the ReaxFF simulation. This result seems somehow to be connected with the difference in the adsorption energies of an adatom in the three distinct binding sites shown in Figure 7, despite that Pt−Pt many-body and entropic effects are not considered in such calculations. The adsorption energies were calculated keeping the graphite lattice frozen while the position of a Pt adatom was optimized with respect to energy. The ReaxFF energy for an adatom adsorbed in the 4-fold coordinated site is much higher than that for the 2-fold coordinated ones. Contrarily, the energy for the 2-fold-coordinated α-site is the highest for the BrennerFF. The significant difference in the coordination number predicted by each of the force fields represents a crucial test to experimentally validate the results obtained. For instance, recent EXAFS experiments have found that the Pt atoms are adsorbed on 4-fold coordinated sites in the interlayer space,[58] which is only compatible with the ReaxFF results. Furthermore, an interlayer position has also been found to be the most stable site for a Pt adatom adsorbed on the armchair edge by electronic structure calculations.[13]
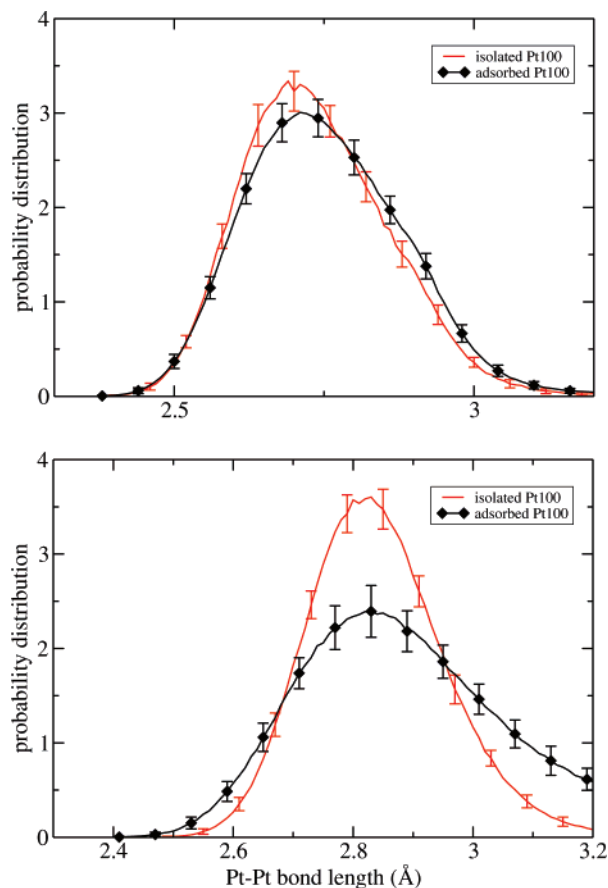

Figure 5. Pt−Pt bond-length distribution for the cluster atoms exposed to the surroundings. (a) Simulation using the BrennerFF. (b) Data from the ReaxFF simulation.

An additional difference between the two force fields is the variation in the number of Pt atoms adsorbed on the graphene layers: 29 atoms are adsorbed on the graphite platelet at the end of the ReaxFF simulation, but only 21 atoms in the case of the BrennerFF. Such a difference in the ultimate number of adsorbed atoms seems to be a result of the relative strength of the interaction between the cluster atoms and the graphite sheets. As shown in Figure 7, the adsorption energy for the most favorable binding site is −123 kcal/mol for the BrennerFF and −251 kcal/mol for the ReaxFF. The BrennerFF adsorption energy is very similar to the BrennerFF energy per atom in the Pt_{100} cluster, −115 kcal/mol, whereas the adsorption energy is lower than the energy per cluster atom, −113 kcal/mol, for the ReaxFF. Therefore, the detachment of cluster atoms and subsequent binding to the graphite sheets are much more energetically favorable for the ReaxFF. Consequently, the entire Pt_{100} cluster flattens during the ReaxFF simulation in close agreement with high-resolution transmission electron microscopy (HRTEM) images[59] (see Figure 8).

To verify the generality of the results described above for the BrennerFF, two more simulations with the BrennerFF, but locating the Pt_{100} cluster on different initial positions over the graphite edge, were carried out. Both simulations led to similar distributions and averages as reported above. In contrast, major restructuring of the atomic positions and the bond-length distribution were observed in a new BrennerFF simulation in which the cluster was initially reoriented with respect to the graphite sheet in such a way that the cluster was only in contact with the substrate by one of its vertices. In this latter case, the cluster increased the contact area by deforming its initial structure. Still the change in the mean bond length was only of
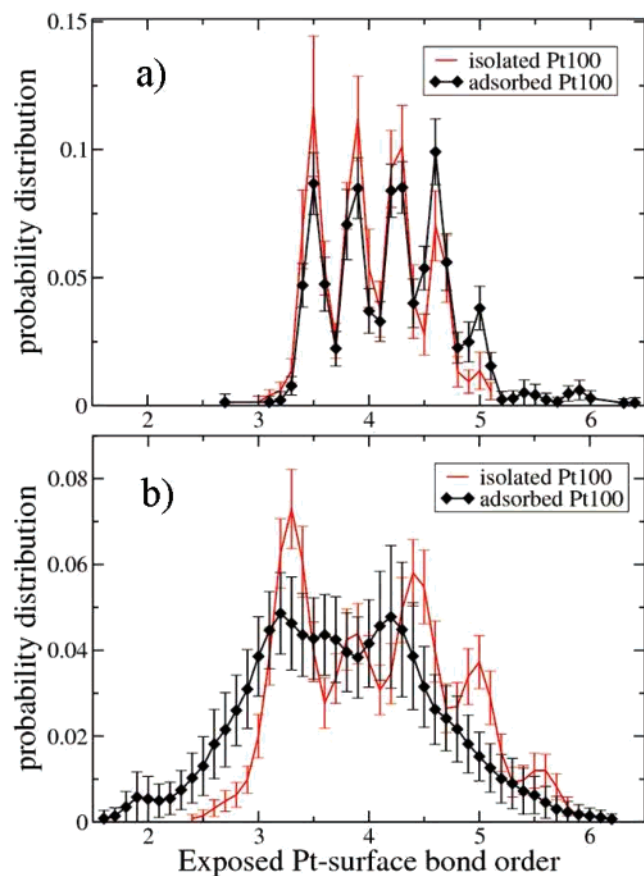
MD of Pt Cluster−C Platelet Interactions

J. Phys. Chem. A, Vol. 112, No. 7, 2008 **1397**

Figure 6. Bond-order distribution for the surface platinum atoms exposed to the surroundings over for both an isolated and an adsorbed Pt_{100} cluster. (a) Simulation using the BrennerFF. (b) Simulation using the ReaxFF.
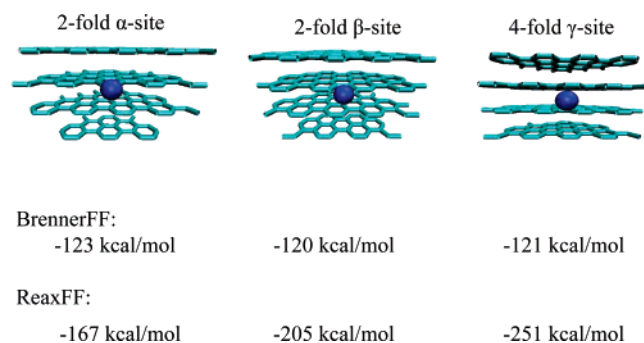

Figure 7. Adsorption energies for a Pt adatom on three distinct binding sites of a graphite armchair edge.

the order of 10^{-4} as a result of a counterbalanced increase in the number of both short and long Pt−Pt bonds. Furthermore, there were no adatoms detached from the cluster and once more the adsorbed Pt atoms moved to 2-fold coordinated positions as occurred with the previous BrennerFF simulations.

Therefore, the ReaxFF reproduces better, at least qualitatively, both the DFT and experimental data available. A priori, both the BrennerFF and ReaxFF could be employed for studies of C−Pt systems. Nonetheless, the available parametrization of the Pt−C BrennerFF[27] has been obtained by mostly fitting DFT data of bulk properties of several C/Pt phases. Apart from dimer properties, no data of finite systems or surfaces have been considered in the parametrization training set and there is therefore no guarantees that the parameters fitted can be transferred to situations where surface effects play a significant role, mainly in compound systems. For example, Murdick et
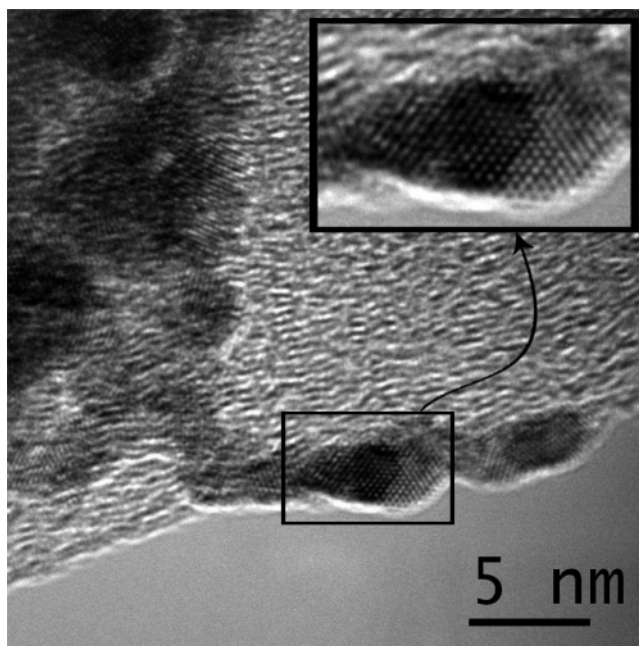

Figure 8. HRTEM image showing the morphology of a platinum cluster adsorbed on the surface of a carbon platelet. Image taken from ref 83.

al. have recently showed that a BrennerFF for Ga−As systems[60] have problems to correctly reproduce ab initio and experimentally observed surface reconstruction.[61,62] In principle, the parametrization of the BrennerFF could be improved by considering DFT data of selected surfaces and finite systems, such as that reported above for the adsorption energy of a Pt adatom. However, it is not trivial to do this and at the same time get the energy of the graphite structure and that of the fcc Pt bulk right in a consistent way, because the BrennerFF depends of a limited number of parameters, many of which are already related to dimer properties. In fact, so far all the available BrennerFF for modeling metal−semiconductor interactions have been parametrized against data for periodic systems. In contrast, the large quantity of parameters and an easier interpretation of the energy terms of the ReaxFF enable the parametrization against a large quantity of DFT data of bulk and surface properties of both periodic and finite systems, thus improving the transferibility of the force field.

The differences observed between the BrennerFF and ReaxFF also highlight the importance of the relative strengh of the graphite−Pt and cluster−Pt interactions to result in the detachment of Pt atoms from the cluster and subsequent flattenning. Because the ReaxFF gives better agreement with the available DFT calculations and experimental observations, we only considered the ReaxFF for further MD simulations.

3.3. Group Analysis of the Bond-Length Distribution. Three normalized bond-length distributions derived from the ReaxFF simulation of a Pt_{100} cluster binding to the armchair edge are presented in Figure 9 for both the Pt−Pt and C−Pt bonds. Apart from the entire cluster, we considered two subsets of Pt atoms as schematically represented by regions I and II in Figure 9a. Regarding the entire cluster, only one pronounced peak is found at ∼2.8 Å for Pt−Pt bonds, whereas two peaks, at ∼2.0 and ∼2.4 Å respectively, are visible for Pt−C bonds in Figure 9b. Metal−carbon bond lengths of both 2.0 and 2.4 Å have also been observed in MD simulations of the catalyzed growth of single-wall carbon nanotubes.[63] On the whole, the Pt−Pt bond-length distribution over the entire cluster is very similar to that found for only atoms at the surface exposed to
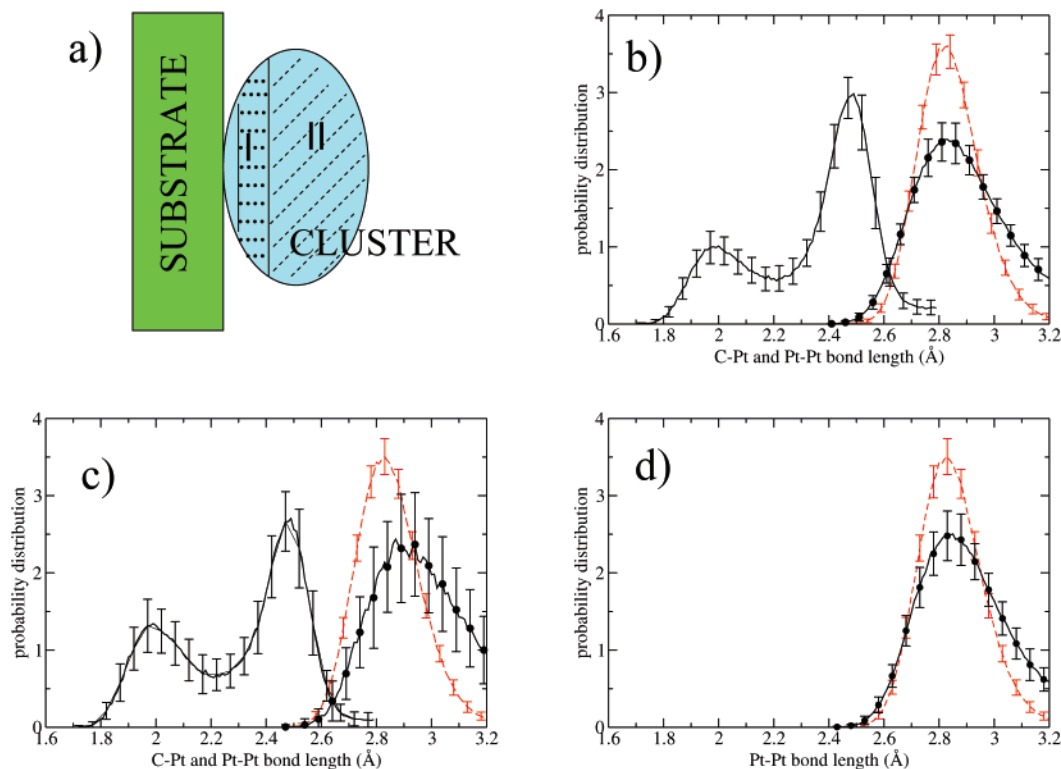
Figure 9. (a) Two different regions of the cluster surface are presented for a detailed analysis of the bond-length distribution. These regions correspond to cluster surface atoms exposed to the environment with a covalent bond with a carbon atom (region I marked by horizontal dotted lines) and with no convalent bonds with carbon atoms (region II marked by oblique dashed lines). (b) Pt−Pt and C−Pt bond-length distribution for the entire cluster. (c) C−Pt and Pt−Pt bond-length distribution for Pt atoms in region I. (d) Pt−Pt bond-length distribution for Pt atom in region II. The discontinuous line represents the Pt−Pt curve for the isolated Pt_{100} cluster, the continuous line with triangles represents the C−Pt curve for an adsorbed Pt_{100} cluster, and the continuous line with circles represents the Pt−Pt curve for an adsorbed Pt_{100} cluster.

the environment (Figure 5b), indicating that the strain propagates over the whole cluster. Nonetheless, the Pt−Pt strain is somewhat larger for the Pt atoms of the exposed surface with covalent bonds with carbon atoms (region I in Figure 9a) as shown in Figure 9c. In the case of the Pt_{100}, we found that a half of the Pt atoms adsorbed to the armchair edge belong to region I. Interestingly, we find, by comparison between parts b and c of Figure 9, that the probability shifts to lower C−Pt bond lengths for Pt atoms at region I. Comparison of Figure 9c,d confirms that the degree of strain is lower for nonadsorbed surface Pt atoms, which may be connected to a different catalytic behavior between regions I and II. It is intriguing that these two regions would give different catalytic activity, which should be investigated in more detail both in experiments and in calculations.

3.4. Electrostatics. Atomic charges using the charge-equilibration scheme in ReaxFF have been investigated for the Pt atoms at the end of the ReaxFF simulation of the binding of the cluster to the armchair edge. We find a small negative charge transfer from the graphite platelet to the platinum cluster. As Figure 10 shows, the largest atomic charge found on a Pt atom is of the order of −0.1 e.

Intriguingly, a small negative charge transfer from the graphite platelet to the platinum cluster is found. Apparently, this seems to be inconsistent with the fact that carbon has a somewhat higher electronegativity than platinum,[64] but the parametrization of the C−Pt electrostatics relies to a large extend on Mulliken charges calculated for C−O and Pt−O. The similar electronegativities between C and Pt as compared to O may thus lead to an uncertainty regarding the relative order of the Pt and C electronegativities in the ReaxFF. Experimentally, information about charge transfer may be deduced from the shift
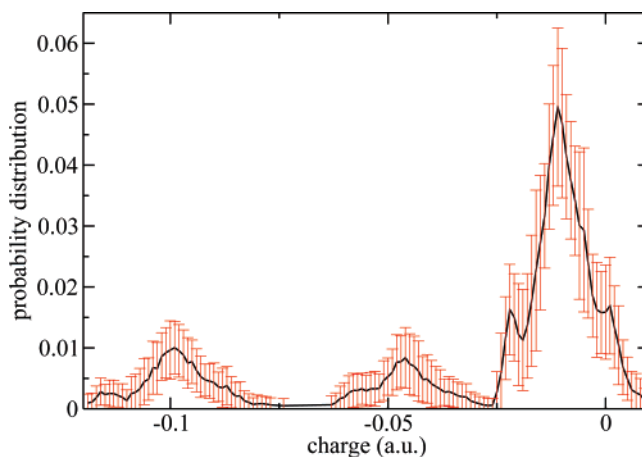

Figure 10. Distribution of atomic charges of the surface atoms of the Pt_{100} cluster adsorbed on the armchair edge.

of core ionization energies in XPS[65] or XANES experiments.[66] However, the shift found experimentally in Pt clusters after being deposited on graphite sheets is very small and cannot give conclusive information without further experimental work.[59]

To quantify the effect of the electrostatics in the ReaxFF simulation, we have first considered the interaction between two probe atoms with an associated charge of 0.1 e each. We find that the ReaxFF interaction between these two charged atoms is screened at Pt−Pt first-neighbor distances (~2.8 Å), but it is negligible at Pt−Pt second neighbor distances, that is, larger than 3.0 Å. Furthermore, a new MD simulation in which the ReaxFF electrostatics terms are turned off gives a similar bond-length distribution to the ReaxFF simulation with electrostatics.
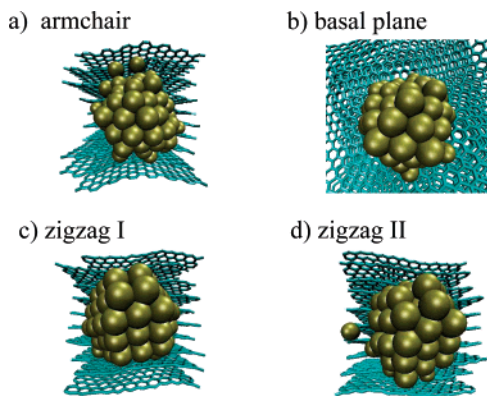
MD of Pt Cluster−C Platelet Interactions

J. Phys. Chem. A, Vol. 112, No. 7, 2008 **1399**

Figure 11. Snapshot taken at the end of the ReaxFF simulation of the Pt_{100} cluster adsorbed on (a) armchair structure, (b) basal plane, and (c, d) two different binding sites of the zigzag structure of the carbon nanosheets.

Therefore, we conclude that the electrostatics has no appreciable effect on simulations of this type of C−Pt systems.

3.5. Binding to Different Carbon−Platelet Edges. Apart from the simulation of the binding to the armchair edge, which will be denoted as "armchair" simulation from now on, we have also performed a few more MD simulations with the ReaxFF to investigate the relation between the local carbon structure and the strain induced in the Pt_{100} cluster. For instance, an MD simulation (denoted by "basal plane" simulation) was performed to model the adsorption of a Pt_{100} cluster on a graphite basal plane, whereas another MD simulation (denoted by "zigzag I" simulation) modeled the Pt_{100} cluster located near the zigzag structure of the graphite platelet. The cluster adsorbed on the graphite basal plane flattened, and the structure of the cluster adsorbed on the zigzag edge remained quasi-intact. To check that not always a Pt_{100} cluster adsorbed on the armchair edge keeps its initial structure, we carried out a second simulation of the binding to the zigzag structure (denoted by "zigzag II" simulation), but in which the center of mass of the cluster was shifted 1.5 Å (i.e., around a half of the graphite interlayer distance) along the direction perpendicular to the graphite plane. This time the cluster structure also flattened. Therefore, a Pt_{100} cluster is susceptible to flattening independently of the graphite edge on where it is adsorbed.

Figure 11 shows a snapshot of the structure of the Pt_{100} cluster at the end of each of the four simulations, showing that, except for the "zigzag I" simulation, the cluster loses its initial structure after adsorption. In addition, Figure 12 confirms that there is no appreciable change in the Pt−Pt bond lengths during the "zigzag I" simulation because its bond-length distribution is quite similar to that of an isolated cluster (Figure 5). In contrast, for the other three cases, Figure 12 clearly shows a considerable increase in the probability of longer Pt−Pt bonds as well as a small increase in the probability of shorter Pt−Pt bonds. Therefore, the net effect of the carbon substrate is to induce a strain in the Pt−Pt distances. Furthermore, as reflected in Figure 13, the number of adsorbed atoms after the equilibration stage in the "zigzag I" case is less than in the other cases. Therefore, the strain induced in the Pt cluster seems to be connected with the number of adsorbed atoms.

The relative positions of the C and Pt atoms in the cluster−platelet interface have been visualized at different times of the MD simulations. Thereby, we have been able to identify some favorable sites, which are presented in Figure 14. As schematically presented in Figure 15, if a Pt atom in contact with the substrate does not occupy at least one of such favorable binding
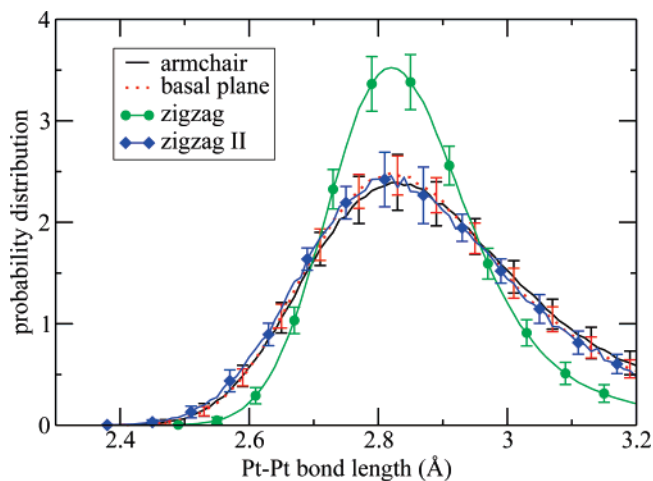

Figure 12. Distribution of the Pt−Pt bond length correspondent to the ReaxFF simulations of the Pt_{100} cluster adsorbed on the armchair structure, basal plane, and the two different binding sites of the zigzag structure of the carbon nanosheets.
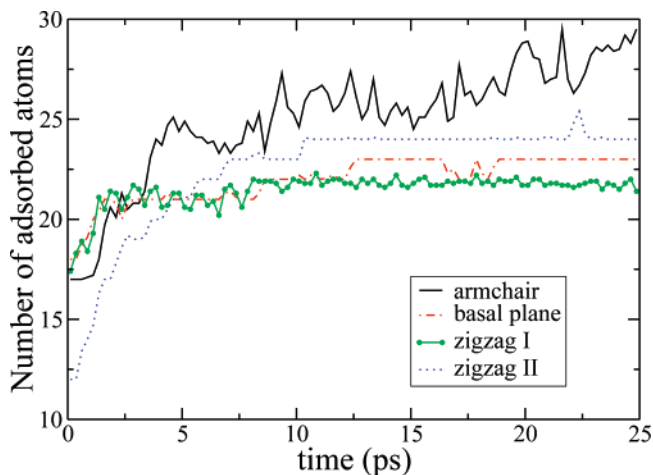

Figure 13. Evolution of the number of adsorbed atoms for each of the MD simulations using the ReaxFF during the equilibration stage.

sites, then it will move to the closest unoccupied site. This migration of cluster atoms across the platelet edge, in turn, open gaps in the cluster−substrate interface. Thus an increasing number of cluster atoms are allowed to come closer to the substrate and then get adsorbed. This explains the increase in the number of adsorbed atoms in Figure 13. The more Pt atoms migrate seeking for a favorable binding site, the more Pt atoms leave their initial positions to become adsorbed on the substrate. Consequently, a flattening of the cluster takes place, leading to a strain in the Pt−Pt bond length. The migratory motion of the cluster atoms occurs differently depending on the nanosheet edge because the Pt atoms are seen to jump to adjacent graphite interlayer gaps in the "armchair" case, whereas cluster atoms bound to the zigzag edge have a preference for moving along one interlayer space. Furthermore, not only the cluster atoms move to find a more stable location but also the substrate monolayers slide against each other to expose η-sites of the armchair and zigzag edges for binding to the cluster atoms. Inspection of the initial atom positions in the "zigzag I" case reveals that most of the Pt atoms in the substrate−cluster interface are located very close to a favorable site and, therefore, they hardly move away from their initial position during the MD simulation. This also, therefore, explains why the Pt atoms are not detached from the cluster during this simulation. Thus the overall structure of the "zigzag I" cluster hardly changes.
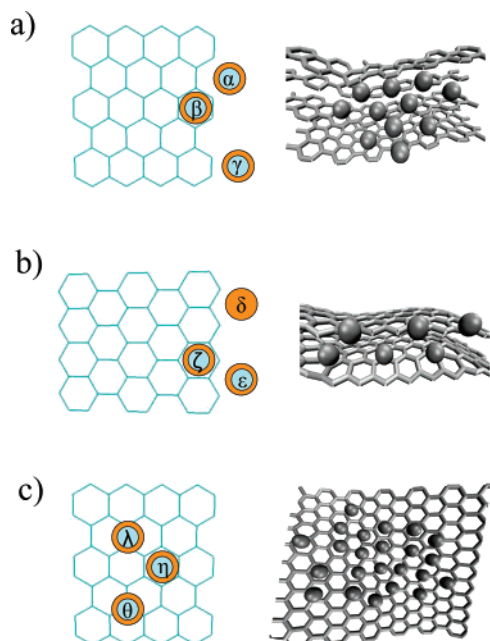
Figure 14. Left: illustration of the favorable sites of the Pt atoms on the three platelet edges found in this work. Each favorable site found in the MD simulations is denoted by a greek letter. A double circle around a greek letter indicates that the center of the mass of the cluster is a few angstroms over the plane of the graphite layer. Right: snapshot of some of the atoms in the platelet−cluster interface taken from the (a) armchair, (b) "zigzag I", and (c) "basal plane" simulations.
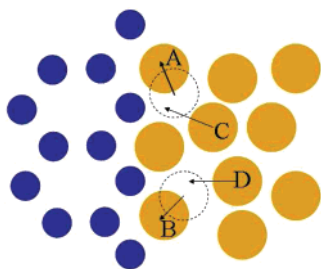

Figure 15. Schematic representation of the restructuring of the cluster atoms (big circles) upon adsorption on a zigzag edge (small circles). Cluster atoms A and B migrate to a more favorable binding site, leaving behind a gap that will then be filled by atoms C and D.

Our observations of adsorbed Pt nanoclusters retaining their initial arrangement as well as flattened clusters are consistent with recent TEM studies,[67] which show both hemispherical and polyhedrally faceted Au clusters supported on carbon nanofibers. It is therefore likely that both zigzag simulations describe real events.

The suggested mechanism is that an initial mismatch in the relative positions of the Pt and C atoms around the platelet−cluster interface plays an important role on the structural changes in the platelet−cluster interface, which are then propagated across the whole cluster. A similar strain effect due to cluster−substrate mismatch has been previously observed in MD simulations of Ag islands on Pt(111)[68] and also suggested from high-resolution scanning electron microscopy (SEM) images of Ag clusters deposited onto graphite.[69]

3.6. Effect of Hydrogen Termination of the Carbon Support. Finally, three more simulations have been carried out adding hydrogen termination to the armchair edge of the carbon platelet. Each of these three new simulations considers a different degree of hydrogen termination. One simulation (denoted "full H termination") modeled the binding of a Pt_{100} cluster to a fully H-terminated carbon platelet. For the other
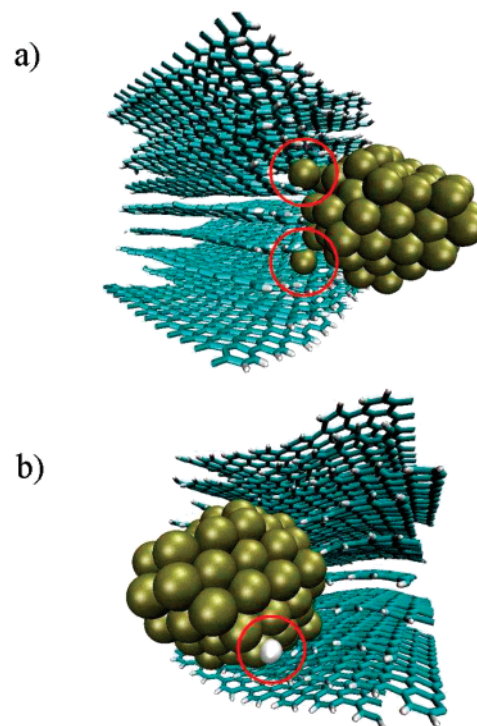

Figure 16. Two different views of the same snapshot of one of the MD simulations with a H-terminated carbon platelet. (a) A couple of platinum atoms (highlighted by a respective circle) are detached from the cluster and moved into the interlayer spacing. (b) a hydrogen atom (highlighted by a circle) was detached from the carbon platelet and diffused inside the Pt cluster until it finally reached a stable position on the cluster surface.

two simulations, the cluster was first located in contact with the substrate. Then the initial configuration of the second simulation (denoted by "partial H termination+") was obtained by hydrogen-terminating the edge carbon atoms that have no covalent bonds with cluster atoms. Finally, for the third simulation ("partial H termination"), first an energy minimization of the substrate−cluster system was performed and then hydrogen atoms were added only to edge carbon atoms with a dangling bond. Thus, in the "partial H termination+" simulation, there were a few more hydrogen atoms than in the "partial H termination" simulation. Similar to the MD simulations with nonterminated edges, some Pt atoms were detached from the cluster, as illustrated in Figure 16. However, this time the detached Pt atoms moved somewhat inside the graphite interlayer spacing because the hydrogen termination prevented such Pt atoms from forming covalent bonds with the C atoms of the platelet edge. On the other hand, a few hydrogen atoms were desorbed from the carbon surface to allow some adsorbed Pt atoms to find more stable positions. These extruded hydrogen atoms diffused across the cluster until they found a more stable position lying on the exposed cluster surface (cf. Figure 16). Interestingly, this is the opposite effect to hydrogen spillover[70] from a nanoparticle to the support suggested by indirect experimental measurements of platinum nanoparticles adsorbed on alumina,[71,72] silica,[73,74] titania,[75] zirconia,[76] zeolite,[77] and carbon-based materials.[78,79] In contrast, the reverse hydrogen spillover found in this work is compatible with DFT and QM/MM studies of supported six-atom clusters of the metals of groups 8 to 11.[80,81]

The new bond-length distributions (Figure 17) lie between that for an isolated cluster and a cluster adsorbed on a nonterminated armchair edge. Thus the hydrogen termination seems to lead to a passivation of the support to some extent.
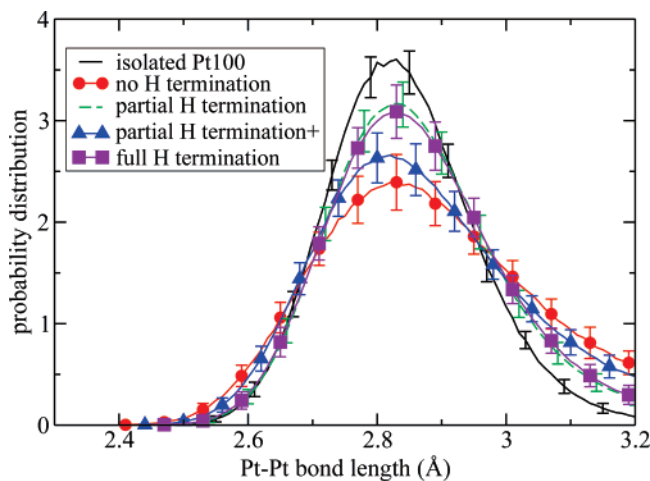
MD of Pt Cluster−C Platelet Interactions

J. Phys. Chem. A, Vol. 112, No. 7, 2008 **1401**

Figure 17. Bond-length distribution for the ReaxFF simulations of the Pt_{100} cluster adsorbed on the armchair edge. The continuous curve with no symbols represents the distribution obtained from data of the ReaxFF simulation of the Pt_{100} cluster adsorbed on the armchair edge without hydrogen termination of the carbon platelet. The remaining curves represent data from the MD simulation of the Pt_{100} cluster adsorbed on three different H-terminated surfaces.

Nonetheless, there is no clear trend in the bond-length distribution with respect to the degree of hydrogen coverage. For example, the bond-length distribution correspondent to the "partial H termination" simulation is more similar to that of the cluster adsorbed on a naked surface than the other two cases with lower and higher degree of hydrogen coverage respectively. This might indicate that, for both the "full H termination" and "partial H termination+" simulations, the variation in the bond length could even get closer to that of a cluster adsorbed on a non-H-terminated edge after much longer time scales. In fact, a larger number of hydrogen atoms might be extruded over time scales much larger than a nanosecond, leaving the cluster in direct contact with the substrate as in the case of a non-hydrogen-terminated surface. At this stage, we can only note that hydrogen termination does not prevent some Pt atoms from being detached from the cluster and occupy more stable positions in graphite interlayer sites and the overall effect is, once more, a flattening of the cluster structure and a subsequent strain in the Pt−Pt bond length.

4. Conclusions

We find that the simulations are able to describe a strain effect similar to that found in experiments of metal clusters on graphite surfaces.[8,69] Such an effect has been successfully connected to the detachment of Pt atoms from the cluster surface to more stable sites on the graphite edges, which, in turn, leads to a flattening of the structure of the Pt cluster. Several optimal binding sites are found depending on the adsorption edge. Still we find that the structure of the cluster can keep its initial structure when there is no significant mismatch between the initial positions of the Pt and C atoms. Hydrogen termination does not prevent the strain effect on the cluster.

References and Notes

(1) Turner, J. A. *Science* **2004**, *305*, 972−974.
(2) Jayaraman, S.; Hiller, A. C. *Mater. Sci. Tech.* **2005**, *16*, 5−13.
(3) Che, G. L.; Lakshmi, B. B.; Fisher, E. R.; Martin, C. R. *Nature* **1998**, *393*, 346−349.
(4) Melechko, A. V.; Merkulov, V. I.; McNight, T. E.; Guillorn, M. A.; Klein, K. L.; Lowndes, D. H.; Simpson, M. L. *J. Appl. Phys.*, 97, Art. no. 041301, 2005.
(5) Lee, K.; Zhang, J.; Wang, H.; Wilkinson, D. P. *Journ. Appl. Electrochem.* **2006**, *36*, 507−522.
(6) Vinodgopal, A. K.; Kuwabata, S.; Kamat, P. V. *J. Phys. Chem. B* **2006**, *110*, 16185−16188.
(7) Tang, J. M.; Jensen, K.; Waje, M.; Li, W.; Larsen, P.; Pauley, K.; Chen, Z.; Ramesh, P.; Itkis, M. E.; Yan, Y.; Haddon, R. C. *J. Phys. Chem. C* **2007**, *111*, 17901−17904.
(8) Ochoa-Fernández, E.; Chen, D.; Yu, Z.; Tøtdal, B.; Rønning, M.; Holmen, A. *Surf. Sci.* 2004, *554*, L107−L112.
(9) Koningsberger D. C.; Gates, B. C. *Chem. Lett.* **2004**, *14*, 271−277.
(10) Nørskov, J. K.; Bligaard, T.; A. Logadottir, S.; Bahn, L. B.; Hansen, M.; Bollinger, H.; Bengaard, H.; Hammer, B.; Sljivancanin, Z.; Mavrikakis, M. Xu, Y.; Dahl, S.; Jacobsen, C. J. H. *J. Catal.* **2002**, *209*, 275−278.
(11) Nilsson, A.; Pettersson, L.; Hammer, B.; Bligaard, T.; Christensen, C.; Nørskov, J. *J. Catal.* **2005**, *100*, 111−114.
(12) Rossmeisl, J.; Logadottir, A.; Nørskov, J. K. *Chem. Phys.* **2005**, *319*, 178−184.
(13) Kong, K.-J.; Choi, Y.; Ryu, B.-H.; Lee, J.-O.; Chang, H. *Mater. Sci. Eng. C.* **2006**, *26*, 1207−1210.
(14) Acharya, C. K.; Turner, C. H. *J. Phys. Chem. B* **2006**, *110*, 17706−17710.
(15) Sokol, A. A.; Bromley, S. T.; French, S. A.; Catlow, R. A.; Sherwood, P. *Int. J. Quantum Chem.* **2004**, *99*, 695−712.
(16) *Combined Quantum Mechanical Methods*; Gao, J., Thompson, M. A., Eds.; Americal Chemical Society: Washington, DC, 1998.
(17) Cao, D.; Feng, P.; Wu, J. *Nano Lett.* **2004**, *4*, 1489−1492.
(18) Shibuta, Y.; Elliot, J. A. *Chem. Phys. Lett.* **2006**, *427*, 365−370.
(19) Tersoff, J. *Phys. Rev. Lett.* **1988**, *61*, 2879−2882.
(20) Brenner, D. W. *Phys. Rev. B* **1990**, *42*, 9458−9471.
(21) Beardmore, K.; Smith, R. *Philos. Mag. A* **1996**, *74*, 1439−1466.
(22) Ni, B.; Lee, K.-H.; Sinnott, S. B. *J. Phys.: Condens. Matter* **2004**, *16*, 7261−7275.
(23) Erhart, P.; Juslin, N.; Goy, O.; Nordlund, K.; Muller, R.; Albe, K. *J. Phys.: Condens. Matter* **2006**, *18*, 6585−6605.
(24) Juslin, N.; Erhart, P.; Traskelin, P.; Nord, J. K.; Henriksson, O. E.; Nordlund, K.; Salonen, E.; Albe, K. *J. Appl. Phys.* **2006**, *18*, 6585−6605.
(25) Erhart, P.; Albe, K. *Phys. Rev. B* **2005**, *71*, 035211.
(26) Nord, J.; Albe, K.; Erhart, P.; Nordlund, K. *J. Phys.: Condens. Matter* **2003**, *15*, 5649−5662.
(27) Albe, K.; Nordlund, K.; Averback, R. S. *Phys. Rev. B* **2002**, *65*, 195124.
(28) Rappé, A. K.; Goddard, W. A., III. *J. Phys. Chem.* **1991**, *95*, 3358−3363.
(29) van Duin, A. C. T.; Dasgupta, S.; Lorant, F.; Goddard, W. A., III. *J. Phys. Chem. A* **2001**, *105*, 9396−9409.
(30) van Duin, A. C. T.; Strachan, A.; Stewman, S.; Zhang, Q.; Xu, X.; Goddard, W. A., III. *J. Phys. Chem. A* **2003**, *107*, 3803−3811.
(31) Zhang, Q.; Çağin, T.; van Duin, A.; Goddard, W. A., III; Qi, Y.; Hector, L. G., Jr. *Phys. Rev. B* **2004**, *69*, 045423.
(32) Nielson, K. D. A.; van Duin, C. T.; Oxgaard, J.; Deng, W.-Q.; Goddard, W. A., III. *J. Phys. Chem. A* **2005**, *109*, 493−499.
(33) Cheung, S.; Deng, W.-Q. A.; van Duin, C. T.; Goddard, W. A., III. *J. Phys. Chem. A* **2005**, *109*, 851−859.
(34) Han, S. S.; van Duin, A. C. T.; Goddard, W. A., III; Lee, H. M. *J. Phys. Chem. A* **2005**, *109*, 4575−4582.
(35) Goddard, W. A., III; van Duin, A. C.; Chenoweth, T. K.; Cheng, M-J.; Pudar, S.; Oxgaard, J.; Merinov, B.; Jang, Y. H.; Persson, P. *Top. Catal.* **2006**, *38*, 93−103.
(36) Smith, R.; Beardmore, K. M. *Thin Solid Films* **1996**, *272*, 255−270.
(37) Schultz, P. A. Unpublished. A description of the method is in: Feibelman, P. J. *Phys. Rev. B* **1987**, *35*, 2626.
(38) Verdozzi, C.; Schultz, P.; Wu, A. R.; Edwards, A. H.; Kioussis, N. *Phys. Rev. B* **2002**, *66*, 125408.
(39) Perdew, J. P.; Burke, K.; Ernzerhof, M. C. *Phys. Rev. Lett.* **1996**, *77*, 3865−3868.
(40) Hamann, D. R. *Phys. Rev. B* **1989**, *40*, 2980−2987.

(41) Jacob, T.; Muller, R. P.; Goddard, W. A., III. *J. Phys. Chem. B* **2003**, *107*, 9465−9476.

(42) Ludwig, J.; Vlachos, D. G.; van Duin, A. C. T.; Goddard, W. A., III. *J. Phys. Chem. B* **2006**, *110*, 4274−4882.

(43) Becke, A. D. *J. Phys. Chem.* **1993**, *98*, 5648−5652.

(44) Lee, C.; Yang, W.; Parr, R. G. *Phys. Rev. B* **1988**, *37*, 785.

(45) Jaguar 4.2. Schrödinger Inc.: Portland, OR.

(46) Hay P. J.; Wadt, W. R. *J. Phys. Chem.* **1985**, *82*, 270−283.

(47) Sanz-Navarro, C. F.; Kenny, S. D.; Porter, A. R.; Pickles, S. M. *Proc. UK e-Science All Hands Meeting, Nottingham, UK*, available from http://www.allhands.org.uk/2004/proceedings/papers/107.pdf, 2004.

(48) Martyna, G. J.; Klein, M. L.; Tuckerman, M. *J. Chem. Phys.* **1992**, *97*, 2635−2643.

(49) Paulus, P. M.; Goossens, A.; Thiel, R. C.; Schmid, G.; van der Kraan, A. M.; de Jongh, L. J. *Phys. Rev. B* **2001**, *64*, 205418.

(50) Kvande, I.; Briskeby, S. T.; Tsypkin, M.; Hammer, N.; Rønning, M.; Sunde, S.; Chen, D.; Tunold, R. *Top. Catal.*, in press.

(51) Hobday, S.; Smith. R. *J. Chem. Soc., Faraday Trans.* **1997**, *93*, 3919−3926.

(52) *Chemistry: The Central Science*, 10th ed.; Prentice Hall: Upper Saddle River: NY, 2005.

(53) Berendsen, H. J. C.; Postma, J. P. M.; van Gunsteren, W. F.; DiNola, A.; Haak, J. R. *J. Chem. Phys.* **1984**, *81*, 3684−3690.

(54) Faken, D.; Jónsson, H. *Comput. Mater. Sci.* **1994**, *2*, 279−286.

(55) Lopez, N.; Janssens, T. V. W.; Clausen, B. S.; Xu, Y. Mavrikakis, M.; Bligaard, T.; Nørskov, J. K. *J. Catal.* **2004**, *223*, 232−235.

(56) Sanner, M. F.; Olson, A. J.; Spenher, J.-C. *Biochemistry* **1996**, *38*, 305−320.

(57) Jacob, T.; Goddard, W. A., III. *J. Phys. Chem. B* **2005**, *109*, 297−311.

(58) Zhang, Y.; Toebes, M. L.; van der Eerden, A.; O'Gradi, W. E.; de Jong, K. P.; Koningsberger.D. C. *J. Phys. Chem. B* **2004**, *108*, 18509.

(59) Rønning, M.; et al. Manuscript in preparation.

(60) Albe, K.; Nordlund, K.; Nord, J.; Kuronen, A. *Phys. Rev. B* **2002**, *66*, 035205.

(61) Murdick, D. A.; Zhou, X. W.; Wadley, H. N. G.; Nguyen-Manh, D. *J. Phys.: Condens. Matter* **2005**, *17*, 6123−6137.

(62) Murdick, D. A.; Zhou, X. W.; Wadley, H. N. G. *J. Phys.: Condens. Matter* **2005**, *72*, 205340.

(63) Zhao, J.; Martinez-Limia, A.; Balbuena, P. B. *Nanotechnology* **2005**, *16*, S575−S581.

(64) *Chemical Principles*, 3rd ed.; Benjamin/Cumming Publishing Co. Inc.: Menlo Park, CA, 1979.

(65) *ESCA Applied to Free Molecule*s; North-Holland Publishing Co.: Amsterdam, 1971.

(66) *X-ray Absorption: Principles, Applications, Techniques of EXAFS, SEXAFS, and XANES*; John Wiley & Sons: Amsterdam, 1988.

(67) Hammer, N.; Kvande, I.; Gunnarsson, Xu, X.; Tøtdal, V. B.; Chen, D.; Rønning, M. *Catal. Today* **2007**, *123*, 245−256.

(68) Blandin, P.; Massobrio, C.; Ballone, P. *Phys. Rev. Lett.* **1994**, *72*, 3072−3075.

(69) Goldby, I. M.; Kuipers, L.; von Issendorff, B.; Palmer, R. E. *Appl. Phys. Lett.* **1996**, *69*, 2819−2821.

(70) Pajonk, G. M. *Appl. Catal. A* **2000**, *202*, 157−169.

(71) Stoica M, M.; Caldararu, M.; Rusu, F.; Ionescu, N. I. *Appl. Catal. A* **1999**, *183*, 287−293.

(72) Zhong, X. Y.; Zhu, J.; Liu, J. Y. *J. Catal.* **2005**, *236*, 9−13.

(73) Wallin, M.; Grönbeck, H.; Lloyd-Spetz, A.; Skoglundh, M. *Appl. Surf. Sci.* **2004**, *235*, 487−500.

(74) Kuhlmanna, A.; Roessner, F.; Schwieger, W.; Gravenhorst, O.; Selvam, T. *Catal. Today* **2004**, *97*, 303−306.

(75) Beck D. D.; White, J. M. *J. Phys. Chem.* **1984**, *88*, 2764−2771.

(76) Benvenutti, E. V.; Franken, L.; Moro, C. C.; Davanzo, C. U. *Langmuir* **1999**, *5*, 8140−8146.

(77) Yang, H.; Chen, H.; Chen, J.; Omotoso, O.; Ring, Z. *J. Catal.* **2006**, *243*, 36−42.

(78) Mitchell, P. C. H.; Ramirez-Cuesta, A. J.; Parker, S. F.; Tomkinson, J.; Thompsett, D. *Chem. Phys.* **2003**, *107*, 6838−6845.

(79) Zacharia, R.; Hwanga S. W.; Rathera, S.; Nahm, K. S. *Chem. Phys. Lett.* **2007,** *434*, 286−291.

(80) Vayssilov, G. N.; Rösch, N. *Phys. Chem. Chem. Phys.* **2005**, *7*, 4019−4026.

(81) Shor, E. A. I.; Nasluzov, V. A.; Shor AM, A. M.; Vayssilov, G. N.; Rösch, N. *J. Phys. Chem. C* **2007**, *111*, 12340−12351.

(82) Cleveland, C. L.; Luedtke, W. D.; Landman, U. *Phys. Rev. B* **1999**, *60*, 5065−5077.

(83) Skoe, I. M. MSc thesis, Norwegian University of Science and Technology (NTNU), Norway, 2006.